# Spectral Element Modeling of Semiconductor Heterostructures

G. von Winckel* and S. Krishna†
*Center for High Technology Materials, University of New Mexico, Albuquerque, New Mexico 87131*

E. A. Coutsias‡
*Department of Mathematics and Statistics, University of New Mexico, Albuquerque, New Mexico 87131*

We present a fast and efficient spectral method for computing the eigenvalues and eigenfunctions for a one-dimensional piecewise smooth potential as is the case of epitaxially grown semiconductor heterostructures. Many physical devices such as quantum well infrared photo-detectors rely upon transitions between bound and quasi-bound or continuum states, consequently it is imperative to determine the resonant spectrum as well as the bound states. Two approaches to the unbound domain problem are introduced. A least-squares rational approximation for radiation conditions can give sizeable errors which do not improve with truncation. Instead of trying to approximate the transparent boundary conditions, our method uses mapping to compute the solution over all space to machine precision. Moreover, we demonstrate that the resonant eigenvalues can computed without shooting methods by deforming the coordinates in the complex plane to a contour along which the eigenfunctions decay exponentially. Finally, we introduce a means of computing inner products and expectations of operators with quadrature accuracy in the spectral domain.

PACS numbers: 73.21.-b, 02.60.Lj, 03.65.Ge

## I. INTRODUCTION

Spectral methods have been most popular in the field of computational fluid dynamics[1], although as we shall demonstrate, they are especially well suited to quantum mechanical problems. Even so, the literature for spectral methods in quantum mechanics is relatively limited. More commonly, finite difference[2] schemes or shooting methods such as the transfer matrix[3, 4] and transmission line analogy[5] have been employed in computing eigenvalues and eigenfunctions for quantum mechanical potentials. Spectral methods have been employed to compute eigenfunctions for atomic[6] and oscillator[7] potentials with great success. Here we introduce a spectral-element approach based on Lanczos' tau method[8] for solving the one-dimensional time-independent Schrödinger equation (TISE) with arbitrary piecewise smooth potentials in unbounded domains. This approach allows for a numerically robust and fast computation of the eigenvalues and eigenvectors of the Hamiltonian operator for potentials with an arbitrary number of discontinuities typified by epitaxially grown quantum semiconductor devices. The spectral method offers a substantial advantage over shooting methods in that it is possible to simultaneously compute as many eigenfunctions and eigenvalues as desired. While this is also true for finite difference schemes, we shall see that for a given tolerable error, the spectral method requires matrices which are usually orders of magnitude smaller than the corresponding finite difference matrices. Since the energy band profile of an epitaxially grown structure is piecewise smooth, spectral-element methods guarantee exponential convergence of the solution[10], whereas finite-difference methods will converge only algebraically.

Spectral methods are divided into three general types, Galerkin, tau, and collocation schemes which are also called pseudospectral methods. In the Galerkin method, the solution of a differential equation (DE) is expanded in terms of trial functions. The trial functions are constructed from a basis of orthogonal polynomials so that each trial function satisfies the boundary conditions (BCs) independently. In contrast, the tau method directly uses the basis functions as trial functions even though these do not individually satisfy the BCs. Instead so-called tau conditions are imposed which require that the superposition of trial functions satisfy the BCs. Both tau and Galerkin methods operate in the spectral or modal space, meaning that the solution of the DE is represented by a vector containing the coefficients of expansion in terms of trial functions. Collocation schemes work directly in point or nodal space and are frequently favored for nonlinear problems as the iterative solution to the DE often requires less computational effort. DE's involving complicated BCs can render Galerkin methods less appealing as the construction of trial functions becomes more laborious and computationally expensive. We prefer the tau method over collocation for two reasons. It gives slightly faster convergence, but more importantly the matrices can be converted to quasi-banded form[14, 15] allowing the use of sparse eigenvalue-solvers. We chose Chebyshev polynomials of the first kind as the trial functions because the Chebyshev-Gauss-Lobatto nodes have a closed-form expression and allow use of the Fast Fourier Transform (FFT) to transform between point space and modal space. In general, we found that using Legendre polynomials as the trial functions resulted

*Electronic address: gregvw@chtm.unm.edu
†Electronic address: skrishna@chtm.unm.edu
‡Electronic address: vageli@math.unm.edu

in slightly reduced rates of convergence.

Our multi-domain approach combined with rational mapping allows one to treat the asymptotic regions exactly as any other elements. By deforming the coordinates to a contour in the complex plane, we can find a trajectory along which the resonant eigenfunctions decay and have a convergent expansion which allows the efficient computation of the resonant spectrum.

## II. FORMULATION

The TISE in one dimension is

$$\left\{-\frac{\hbar^2}{2}\frac{d}{dx}\frac{1}{m^*(x)}\frac{d}{dx}+V(x)\right\}\psi(x)=E\psi(x) \tag{1}$$

Assume that $V'(x)$ has compact support such that the potential is asymptotically constant.

$$V(x)=\begin{cases} V_l & \text{if} \quad x<x_l \\ V_r & \text{if} \quad x>x_r \end{cases} \tag{2}$$

The potential $V(x)$ may have discontinuities at $x_l$ and $x_r$ but is assumed smooth for $x_l < x < x_r$. Let

$$p(x)=\frac{m_0}{m^*(x)}, \quad q(x)=\frac{2m_0}{\hbar^2}V(x), \quad \lambda=\frac{2m_0}{\hbar^2}E \tag{3}$$

and we get the Sturm-Liouville equation.

$$\left\{-\frac{d}{dx}p(x)\frac{d}{dx}+q(x)\right\}\psi(x)=\lambda\psi(x) \tag{4}$$

A linear transformation maps from the interval $x \in [x_l, x_r]$ to the unit interval $\tilde{x} \in [-1, 1]$. This transformation is

$$\tilde{x}=\frac{2x-x_l-x_r}{x_r-x_l}, \quad u(\tilde{x})=\psi(x) \tag{5}$$

The Schrödinger eigenproblem is then solved numerically using Lanczos' tau method[8] which is described in detail below. Let $N$ be the order of truncation so that on the unit interval the Chebyshev-Gauss-Lobatto (CGL) nodes are

$$\tilde{x}_k=\cos\frac{\pi k}{N}, \quad k\in\{0,1,...,N\} \tag{6}$$

The known functions $p(\tilde{x})$ and $q(\tilde{x})$ are samples at the CGL nodes and are expanded in terms of Chebyshev polynomials of the first kind[10]

$$p_N(\tilde{x})=\sum_{j=0}^{N}\hat{p}_j T_j(\tilde{x}) \ . \tag{7}$$

The Chebyshev polynomials satisfy the following recurrence relation and derivative identity[11]

$$\begin{aligned} T_0(x)=1, \quad T_1(x)=x \ , \\ T_{j+1}(x)=2xT_j(x)-T_{j-1}(x) \ , \\ 2T_j(x)=\frac{1}{j+1}T'_{j+1}(x)-\frac{1}{j-1}T'_{j-1}(x) \ . \end{aligned} \tag{8}$$

The values that $p(\tilde{x})$ takes at the CGL nodes are stored in a column vector $\mathbf{p}_N$. The vectors of nodal values and expansion coefficients are related by the cosine transform matrix

$$\mathbf{p}_N=\mathbf{M}\hat{\mathbf{p}}, \quad M_{ij}=\cos\frac{\pi ij}{N} \tag{9}$$

The structure of the matrix $M$ allows for transformation between the nodal space where the function is represented by the vector $\mathbf{p}_N$ and the coefficient space where the function is represented by $\hat{\mathbf{p}}$ using the FFT which scales as $O(N\log(N))$ instead of $O(N^2)$. The functions $p(x)$, $q(x)$ and $w(x)$ have convolution matrix representations[14] of the form

$$\mathbf{P}=\sum_{j=0}^{N}\hat{p}_j\mathbf{T}_j \ , \tag{10}$$

where the $\mathbf{T}_j$ are computed from the Chebyshev recurrence relation applied to the $\mathbf{X}$ matrix (A2)

$$\begin{aligned} \mathbf{T}_0=\mathbf{I} \ , \quad \mathbf{T}_1=\mathbf{X} \ , \\ \mathbf{T}_{j+1}=2\mathbf{X}\mathbf{T}_j-\mathbf{T}_{j-1} \ , \ j=1,2,\ldots \end{aligned} \tag{11}$$

Here $\mathbf{I}$ is the identity. One now obtains the matrix form of the differential equation

$$\left\{-\alpha^2\mathbf{D}\left[\mathbf{P}\mathbf{D}\right]+\mathbf{Q}\right\}\hat{\mathbf{u}}=\lambda\hat{\mathbf{u}} \ . \tag{12}$$

where the differentiation operator has discretized as the $\mathbf{D}$ matrix (A1). The $\alpha$ term is a scaling factor which arises from the change of coordinates when the problem was mapped onto the unit interval ($\alpha = 2/L$). It is often desirable to convert to integration preconditioned form[15], which improves the convergence, but more importantly renders the generalized eigenproblem more sparse, which is of particular value when using a sparse eigenvalue solver such as ARPACK[16]. Two important identities are

$$\mathbf{D}\mathbf{X}-\mathbf{X}\mathbf{D}=\mathbf{I}, \quad \mathbf{B}_{[1]}\mathbf{D}=\mathbf{I}_{[1]} \ . \tag{13}$$

where $\mathbf{B}_{[1]}$ is the integration matrix (A3). We use the notation $\mathbf{A}_{[n]}$ for the matrix $\mathbf{A}$ with the first $n$ rows set to zero. To convert to integrator form, the second derivative must be brought to the left of $\mathbf{P}$ to do so, the necessary identity is

$$\mathbf{P}\mathbf{D}=\mathbf{D}\mathbf{P}-\mathbf{P}' \ , \tag{14}$$

where the prime notation indicates

$$\mathbf{P}'=\sum_{j=0}^{N}\hat{p}'_j\mathbf{T}_j, \quad \hat{\mathbf{p}}'=\mathbf{D}^\top\hat{\mathbf{p}} \ . \tag{15}$$

The DE is rewritten as the matrix equation

$$\left\{-\alpha^2\mathbf{D}\left[\mathbf{D}\mathbf{P}-\mathbf{P}'\right]+\mathbf{Q}\right\}\hat{\mathbf{u}}=\lambda\hat{\mathbf{u}} \tag{16}$$

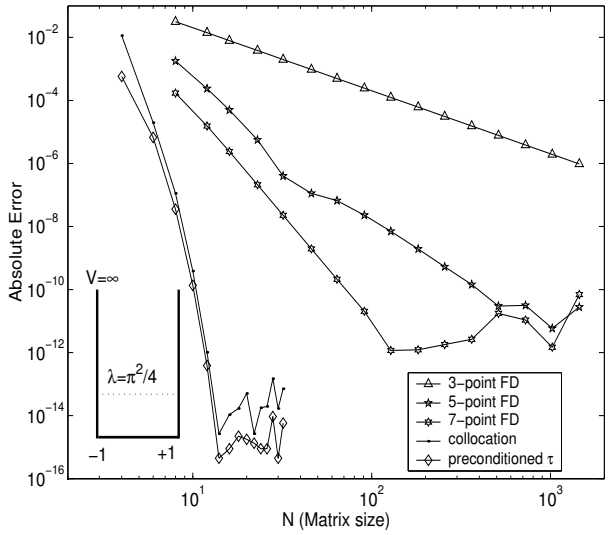


FIG. 1: Convergence comparison of the tau, collocation, and finite difference methods for the ground state of the infinite potential well of width $L = 2$ (unitless).

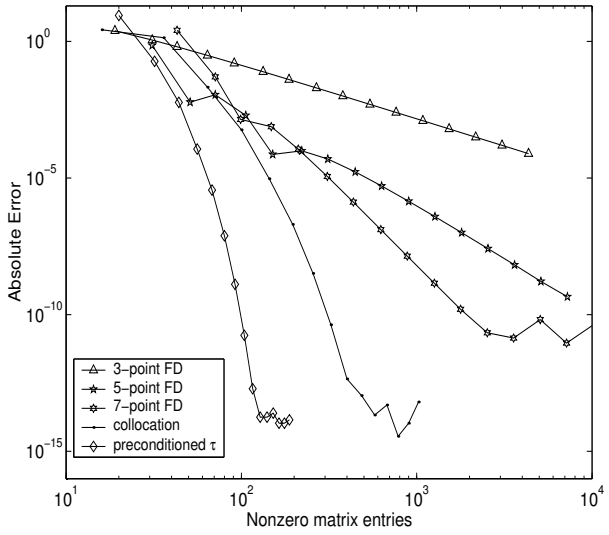


FIG. 2: Comparison of spectral and finite difference methods for the convergence of the third eigenvalue as a function of number of nonzero matrix elements.

The integration $\mathbf{B}_{[1]}$ matrix is then applied twice and letting

$$\mathbf{L} = -\alpha^2\mathbf{P} + \alpha^2\mathbf{B}\mathbf{P}' + \mathbf{B}^2\mathbf{Q} \tag{17}$$

we obtain the generalized eigenvalue problem (GEP)

$$\mathbf{L}\hat{\mathbf{u}} = \lambda\mathbf{B}^2\hat{\mathbf{u}} \ . \tag{18}$$

Now we must impose the two tau conditions since the DE is second order. This is accomplished by inserting Dirichlet operators for the endpoints into the first two rows of $\mathbf{L}$. These operators are described below. The GEP is solved numerically using the QZ algorithm[9]. This is done easily in MATLAB®with the command `eig(L,B2)`.

To demonstrate the convergence, we show the absolute error versus polynomial truncation for an infinite potential well on the unit interval. The convergence of the tau, collocation, and finite difference (FD) schemes for the ground state makes the advantage of spectral methods immediately apparent. The finite difference method, however, exhibits algebraic convergence. For example, the three-point FD scheme has second order convergence. This means that if one doubles the number of FD nodes then the error is expected to reduce by a factor of four. In contrast, the error for tau and collocation spectral methods appears to drop by roughly an order of magnitude for each extra term added to the series and demonstrates the expected exponential convergence.Figure 1 demonstrates the convergence of the integration-preconditioned tau method and collocation method with thee-, five-, and seven-point FD schemes. One advantage of FD schemes is that although the matrix may be very large, it generally has banded or quasi-banded form, consequently the matrix tends to be sparse. The discretized potential will only affect the diagonal elements of the FD and collocation matrices so the sparsity will not be affected as in the case of the tau method. With the availability of sparse solvers[16], perhaps a fairer comparison of the spectral and FD schemes is convergence as a function of matrix sparsity. Figure 2 demonstrates that the tau method not only has a substantial advantage over all three FD schemes, but its advantage over collocation has increased as well. As long as the potential can be closely approximated by a low order polynomial or rational function, as is the case with semiconductor heterostructures, the preconditioned tau method will result in sparse quasi-banded matrices, whereas collocation results in full matrices. The FD approximations were performed on the uniform grid points. Had we chosen the CGL nodes for constructing the FD matrix, then in the limit as the number of points approaches the size of the matrix, the FD matrix would converge to the Chebyshev collocation matrix[12].

## III. MULTIPLE ELEMENTS

While the spectral method produces optimal results approximating smooth functions, in most practical heterostructures, the potential is only smooth within a given epitaxial layer with potential discontinuities in the band edge corresponding to material interfaces. Chebyshev polynomials will converge to a discontinuous function in the $L_2$ sense but not in $L_\infty$ due to the Gibbs phenomenon[10]. Although there exist methods for filtering out the Gibbs phenomena[13] and restoring spectral convergence, heterostructure problems are most efficiently solved using spectral elements since the discontinuities have known fixed locations. When there are multiple elements, there is a different discretized Hamil-

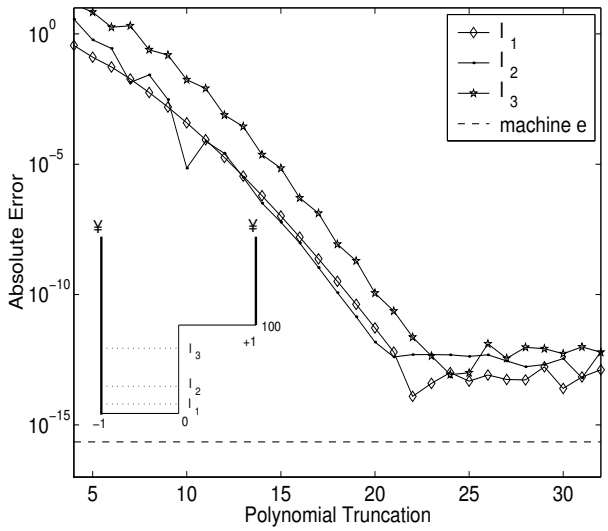


FIG. 3: Absolute error for the first three eigenvalues for the two-element potential well. The exact values were computed with the secant method.

tonian operator for each element. A global solution is obtained by requiring that each local solution and its derivative equal next local solution at the interface between elements. Consider a discontinuous potential well

$$q(x) = \begin{cases} q_1 & : \quad -1 \le x < 0 \\ q_2 & : \quad 0 \le x \le 1 \\ \infty & : \quad |x| > 1 \end{cases} \tag{19}$$

letting for example $q_1 = 0$ and $q_2 = 100$. This gives two DEs where the solutions are coupled through boundary conditions at $x = 0$.

$$\left\{ -\frac{d^2}{dx^2} + q_{1,2} \right\} u_{1,2}(x) = \lambda u_{1,2}(x) \tag{20}$$
$$u_1(-1) = 0, \quad u_2(+1) = 0$$
$$u_1(0) = u_2(0), \quad u_1'(0) = u_2'(0)$$

Since both elements have unit length, the scaling factor is $\alpha = \frac{2}{L} = 2$. Writing (20) in terms of (18)

$$\mathbf{L}_{1,2}\hat{\mathbf{u}}_{1,2} = \lambda \mathbf{B}^2 \hat{\mathbf{u}}_{1,2} \tag{21}$$
$$\boldsymbol{\delta}_- \hat{\mathbf{u}}_1 = 0, \quad \boldsymbol{\delta}_+ \hat{\mathbf{u}}_2 = 0$$
$$\boldsymbol{\delta}_+ \hat{\mathbf{u}}_1 - \boldsymbol{\delta}_- \hat{\mathbf{u}}_\mathbf{2} = 0$$
$$\alpha\boldsymbol{\nu}_+ \hat{\mathbf{u}}_1 - \alpha\boldsymbol{\nu}_- \hat{\mathbf{u}}_\mathbf{2} = 0$$

The Dirichlet and Neumann operators are row vectors defined in (A4). Typically the elements will not be of the same length and the effective mass in the two regions may be different, so the Neumann operators must be scaled accordingly. Now the equations in (21) can be written as a GEP.

$$\left(\begin{array}{c|c} \boldsymbol{\delta}_- & 0 \\ \boldsymbol{\delta}_+ & -\boldsymbol{\delta}_- \\ \hline \mathbf{L}_1 & 0 \\ \hline 0 & \boldsymbol{\delta}_+ \\ -\boldsymbol{\nu}_+ & \boldsymbol{\nu}_- \\ 0 & \mathbf{L}_2 \end{array}\right) \left(\begin{array}{c} \hat{\mathbf{u}}_1 \\ \hline \\ \hline \hat{\mathbf{u}}_2 \end{array}\right) = \lambda \left(\begin{array}{c|c} \mathbf{B}^2_{[2]} & 0 \\ \hline 0 & \mathbf{B}^2_{[2]} \end{array}\right) \left(\begin{array}{c} \hat{\mathbf{u}}_1 \\ \hline \hat{\mathbf{u}}_2 \end{array}\right) \tag{22}$$

This approach generalizes to any number of elements where matching conditions on the solution and its derivative are imposed at the interfaces. In general, the left matrix of the pencil (22) will be block tridiagonal and the right matrix will be block diagonal. Figure 3 compares the first three eigenvalues of (22) with those obtained using the secant method. It should also be mentioned that although we have chosen the same polynomial truncation for each element, this is by no means necessary. Typically one may wish to use a larger truncation with longer elements or in elements where the wavefunction is expected to oscillate rapidly over space. privelage

## IV. UNBOUNDED DOMAINS

A radiation condition is constructed by imposing a Dirichlet-to-Neumann condition which depends on the group velocity. The Schrödinger equation is parabolic because it is first order in time and second order in space, therefore the group velocity has a square root dependence on the electron's energy. The square root function has a branch point at zero kinetic energy, therefore it does not have a convergent Taylor series at this point. One approach to construct radiation conditions for the TISE is to approximate the group velocity by a linear least-squares fit[2]. While this simplifies the problem greatly, we have found that the computed eigenvalues can be off by as much as 20%. Other authors have used Padé approximations [17] of the group velocity with slightly improved results. In the special case of the potential which has the same asymptotic value on both sides, one can write exact radiation conditions by taking the wavenumber as a linear eigenvalue and the energy as a quadratic eigenvalue term[18]. The quadratic eigenvalue problem leads to a doubling of matrix size and is rather limited in usefulness due to the requirement of asymptotic symmetry. Approximate absorbing boundary conditions are developed in detail in section III-A below. Instead of trying to approximate the radiation condition, we demonstrate a method to compute the entire solution over all space to machine precision.

First we consider bound states where the outgoing waves are simple decaying exponentials. A common approach would be to simply truncate the domain at a large distance from the well with the expectation that the wavefunction will have decayed to approximately zero by reaching the endpoint. We shall see, however, that this approach is not optimal as the nodes will be over-clustered where the solution goes to zero. A much more

efficient approach is to use a polynomial expansion on the semi-infinite interval. This has been accomplished with great success using Laguerre functions[19, 20] and it is possible to use multiple families of polynomials in the construction of multi-element operators such as is (22). However, the Laguerre functions are not polynomials and consequently the matrix representations of operators are full matrices and are more computationally expensive to construct. If we wished to compute solutions on finite-length intervals with Chebyshev polynomials and use Laguerre functions for semi-infinite intervals, then we require two sets of operators to solve the complete problem. An attractive alternative is to employ rational mapping [21] which allows one to map the semi-infinite interval to the unit interval while using the same Chebyshev approach as before. Such a mapping results in a clustering of nodes at the interface to the local solution and gives spectral convergence to solutions which decay exponentially.

### A. Absorbing Boundary Conditions

A traditional way to solve DE's on unbounded domains is to truncate the domain and match the numerically computed local solution to a known asymptotic solution[2, 17]. For the TISE in one dimension, this is accomplished by imposing continuity of the logarithmic derivative of the wavefunction across the interface between the local and asymptotic regions. Since the asymptotic solution is of the form $\exp(\sqrt{\lambda - q}x)$, the logarithmic derivative at the interface is some constant times $\sqrt{\lambda - q}$. This term is simply a scaled group velocity. Since the overall eigenproblem depends on both $\lambda$ and $\sqrt{\lambda}$ we can not, in general solve exactly. If, however, the eigenproblem contains only powers of $\lambda$ then it can be solved as a GEP by constructing the companion matrices[18].

We extended the approach of Shibata[2] by approximating the scaled square-root function $\sqrt{1-\phi}$ for $\phi \in [0,1]$ by a least-squares rational function.

$$\sqrt{1-\phi} \approx R(\phi) \equiv \frac{\sum_{k=0}^{K} a_k \phi^k}{1 + \sum_{k=1}^{K} b_k \phi^k} = \frac{\mathcal{A}(\phi)}{\mathcal{B}(\phi)} \qquad (23)$$

The expansion coefficients can be computed exactly by solving the system of equations

$$\nabla_{\vec{a},\vec{b}} \int_0^1 \left( \mathcal{A}(\phi) - \sqrt{1-\phi}\mathcal{B}(\phi) \right)^2 d\phi = \vec{0} \qquad (24)$$

These optimal coefficients are given in table I. Using these various expansions, the error $|R(\phi) - \sqrt{1-\phi}|$ is plotted in figure 4. As one might expect the error decreases through most of the interval for higher order expansions, however, the error does not improve significantly in the neighborhood of the branch point at $\phi = 1$. Although the error appears to be reasonably small, the DE is weakly ill-posed[17] with respect to these approximate BCs. To demonstrate, we computed the seven bound states of a finite potential well on the unit interval with scaled depth of 100. The minimum and maximum relative error for the computed eigenvalues is given in table II. Whether one might desire to use these absorbing boundary conditions depends largely on the required accuracy and nature of the problem. This approach is reasonably suited for finding approximate eigenvalues far away from the top of the quantum well since the rational approximant fits the exact function more closely there. The problems with absorbing boundary conditions can be avoided entirely by solving the TISE over all space. This technique is introduced in the next section.

TABLE I: The coefficients of the first three least-squares rational approximations to the square root function

| | bi-linear | bi-quadratic | bi-cubic |
|---|---|---|---|
| $a_0$ | 0.98674351585014 | 0.99953973549047 | 0.99998457979265 |
| $a_1$ | -0.91988472622478 | -1.67601451666117 | -2.38532812936857 |
| $a_2$ | ··· | 0.68013245842345 | 1.82014806012346 |
| $a_3$ | ··· | ··· | -0.43463829207320 |
| $b_1$ | -0.52449567723343 | -1.18441536224446 | -1.88583012408147 |
| $b_2$ | ··· | 0.24557351809084 | 1.00597708415993 |
| $b_3$ | ··· | ··· | -0.11510707954682 |

TABLE II: Minimum and maximum relative error of the seven bound state eigenvalues for least-squares rational approximations

| | bi-linear | bi-quadratic | bi-cubic |
|---|---|---|---|
| min error | 1.2323% | 0.7585% | 0.3647% |
| max error | 16.1008% | 11.4503% | 14.7714% |

### B. Rational Mapping for Bound States

Now we consider an approach which maps the semi-infinite intervals $(-\infty, -R]$ and $[+R, \infty)$ to the unit interval. This is accomplished using a rational map. Let $y_- : [-\infty, -R] \mapsto [-1, 1]$ and $y_+ : [+R, +\infty] \mapsto [-1, 1]$ These maps and their inverses are

$$y_\pm = \pm 2 \left( \frac{x \mp R}{x \pm R} \right) \mp 1, \quad x = R \frac{y_\pm \pm 3}{1 \mp y_\pm} \qquad (25)$$

The mapped derivatives are

$$\frac{\partial}{\partial x} = \frac{1}{4R}(y_\pm \mp 1)^2 \frac{\partial}{\partial y_\pm} \qquad (26)$$

$$\frac{d^2}{dx^2} = \frac{1}{8R^2}(y_\pm \mp 1)^3 \frac{d}{dy_\pm} + \frac{1}{16R^2}(y_\pm \mp 1)^4 \frac{d^2}{dy_\pm^2} \qquad (27)$$

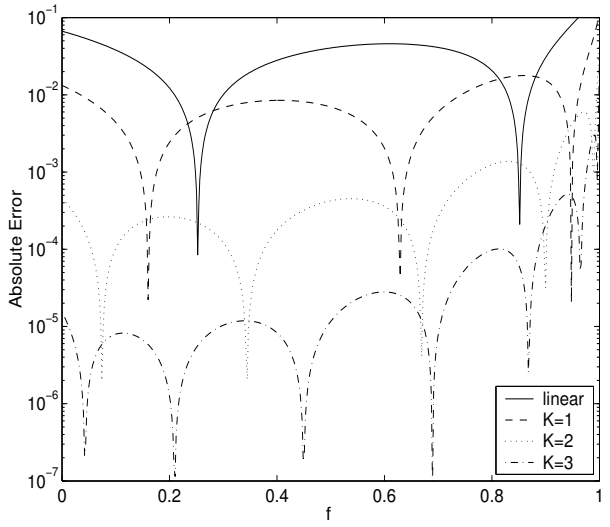


FIG. 4: Absolute error for the linear, bi-linear, bi-quadratic, and bi-cubic least-squares approximations to $\sqrt{1-\phi}$.

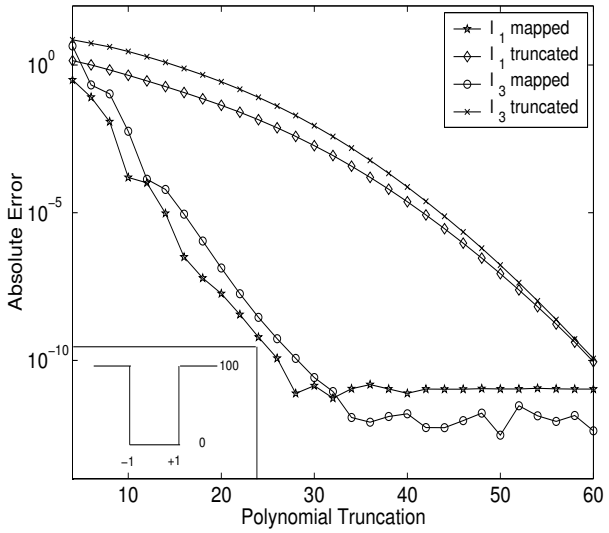


FIG. 5: Absolute error of the first and third eigenvalues with rational mapping compared to domain truncation. For domain truncation, $L = 15$.

One can then construct a three-element scheme similar to (22) where there will be one sub-matrix each for the right and left asymptotic regions and a sub-matrix for the quantum well element. The matching of the Dirichlet conditions and Neumann conditions are exactly as before because the mappings are precisely linear at the points $x = \pm R$. We then implement this approach and examine the convergence of the first and third eigenvalues of a finite potential well with depth $q_0 = 100$ and width $L = 2$. The integrator preconditioned operators for the left (-) and right (+) asymptotic regions are

$$\mathbf{L}_\pm = -\frac{1}{16R^2}(\mathbf{X} \mp \mathbf{I})^4 + \frac{3}{8R^2}\mathbf{B}(\mathbf{X} \mp \mathbf{I})^3 + \mathbf{B}^2[q_0\mathbf{I} - \frac{3}{8R^2}(\mathbf{X} \mp \mathbf{I})^2] \quad (28)$$

whereas the operator for the quantum well is simply $-\mathbf{I}$. The left-hand side of the resulting matrix pencil is

$$l.h.s. = \left(\begin{array}{c|c|c} \boldsymbol{\delta}_- & & \\ \boldsymbol{\delta}_+ & -\boldsymbol{\delta}_- & \\ \mathbf{L}_- & & \\ \hline \boldsymbol{\nu}_+ & -\boldsymbol{\nu}_- & \\ & -\boldsymbol{\nu}_+ & \boldsymbol{\nu}_- \\ & -\mathbf{I} & \\ \hline & -\boldsymbol{\delta}_+ & \boldsymbol{\delta}_- \\ & & \boldsymbol{\delta}_+ \\ & & \mathbf{L}_+ \end{array}\right) \quad (29)$$

and the right-hand-side is simply block diagonal with three $\mathbf{B}^2_{[2]}$ blocks. The exact eigenvalues have been computed using the Newton-Raphson method. Additionally we have computed $\lambda_{1,3}$ using domain truncation where an element of length $L = 15$ has been placed on either side of the quantum well. Figure 5 demonstrates that both methods converge, however the rational map gives spectral convergence whereas the truncated domain approach provides algebraic convergence. Both methods are limited to the calculation of bound states as the Dirichlet conditions imposed by domain truncation will discretize the continuous spectrum into real bound states and destroying the resonances [22–25]. The rational mapping does not work for unbound states since it will map a function which oscillates periodically on an infinite interval to a finite interval thereby creating a function which has an essential singularity at a point in the domain such as $\sin(1/x)$ and can not be approximated using spectral methods. For unbound states we shall take a different approach.

### C. Computing Resonances with Complex Coordinate Deformations

The resonances in the continuum density-of-states (DOS) correspond to the poles of the single-particle Green's function which lie off of the real axis[22]. These eigenvalues do not correspond to physical states as their eigenfunctions exhibit unbounded growth at infinity. Nevertheless, numerous calculations for transitions between bound states and the continuous spectrum depend on the spectral density of unbound states. One can always obtain the DOS from the trace of the Green's function[26] if it is available. commitee

$$\rho_{1D}(\lambda) = \sum_n \delta(\lambda - \lambda_n) = -\frac{1}{\pi}\Im[Tr\{G(x,x';\lambda)\}] \quad (30)$$

For one-dimensional problems a "closed form" for the Green's function can be obtained[27] from solving the boundary value problem using shooting methods[5], however, even constructing just the diagonal elements of the Green's function is unnecessarily expensive as we need

only know the location of the poles[22].

If the coordinate $x$ is taken along the real axis, the eigenfunctions diverge at large distances. Since the coordinates are not a quantum mechanical observable, the spectrum is not affected by solving the eigenvalue problem along a different contour in the complex plane[28]. In general, computation along a contour in the complex plane requires analytically continuing the potential in the complex. However, in the asymptotic region where the potential is constant, this continuation is trivially accomplished. By choosing a new coordinate contour of the form[29, 30]

$$z = \begin{cases} x - ic(-x-R)^n & \text{if} \quad x < -R \\ x & \text{if} \quad -R < x < +R \\ x + ic(x-R)^n & \text{if} \quad x > +R \end{cases} \qquad (31)$$
$$c \in \mathbb{R}^+, \quad n \in \{2, 3, 4, \dots\}$$

the resonant eigenfunctions will exhibit super-exponential decay along the contour. Since the contour is at least $C^1$, there will be no reflection. Consequently, only the resonant eigenvalues with negative imaginary part will be resolved since they correspond to outward propagating solutions. To compute the eigenfunctions along the new contour, all that is required is the modification of the Hamiltonian to the new coordinates.

$$\frac{d^2}{dz^2} = -\frac{d^2 z}{dx^2}\left(\frac{dz}{dx}\right)^{-3}\frac{d}{dx} + \left(\frac{dz}{dx}\right)^{-2}\frac{d^2}{dx^2} \qquad (32)$$

Convergence depends on the choice of the parameters $n$ and $c$. For low energy resonances, $n = 2$ and $c = 1$ give optimal convergence, however, for higher energy states, the solution does not decay fast enough to resolve the eigenfunctions. In these cases, using a cubic or quartic deformation ($n = 3, 4$) or larger coefficient $c$ will make it possible to resolve higher energy states at the expense of requiring higher truncation for the lower states.

The convergence for bound states was shown (Fig. 5) to improve by mapping the semi-infinite interval onto the finite interval, so the same approach can be applied here. The rational map gives the best convergence for functions which decay exponentially[1], however, if we use a quadratic deformation of the coordinates, the resonant eigenfunctions will decay as $e^{-x^2}$. For this type of decay the rational mapping will over-resolve the eigenfunctions away from the local solution. An asymptotically linear deformation will give exponential decay and therefore faster convergence, but will not be globally $C^1$ unless we introduce an matching curve such as in the contour in figure 7, requiring the introduction of intermediate, "matching" elements.

### D. Scattering States and Tunneling

Scattering states belong to the continuous spectrum and for a one-dimensional problem, they can be thought

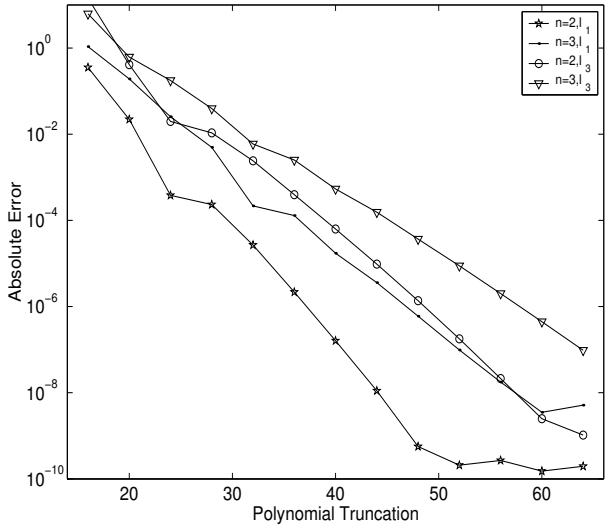


FIG. 6: Convergence of the first and third resonances using quadratic ($n = 2$) and cubic ($n = 3$) contours with end element lengths $L = 2$ and contour coefficient $c = 5$. See equation (31).

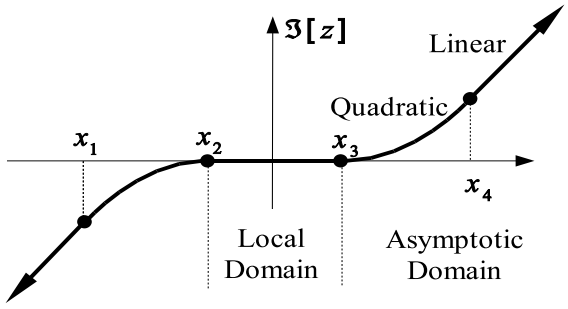


FIG. 7: A $C^1$ contour along which the solutions have asymptotic exponential decay.

of as right or left propagating waves. Unlike resonances, scattering states are physical solutions, but are not true eigenfunctions since the do not satisfy two-point boundary conditions. Traditionally, the scattering states and tunneling probability have been computed using shooting by approximating the potential as piecewise constant[3] or linear[4]. Here we use the same approach, except that the spectral method is optimal because instead of approximating the potential as piecewise constant or linear, any piecewise smooth function allowed.

Here we describe how to compute the right-propagating scattering wavefunction for a single element. Generalization to multiple elements is similar to the eigenvalue problems before and can be solved rapidly since it is a block-tridiagonal system. The initial values for the problem are imposed at the right endpoint. Using the scaled functions and parameters as before

$$u(+1) = 1, \quad u'(+1) = ik_r, \quad k_{r,l} = \sqrt{\lambda - q_{r,l}} \qquad (33)$$

To compute the Chebyshev expansion coefficients for the solution, one must solve the integration-preconditioned system

$$\begin{pmatrix} \boldsymbol{\delta}_+ \\ \boldsymbol{\nu}_+ \\ -\mathbf{I} + \mathbf{B}^2[\mathbf{V} - \lambda\mathbf{I}] \end{pmatrix} \hat{\mathbf{u}} = \begin{pmatrix} 1 \\ ik_r \\ \mathbf{0} \end{pmatrix} \tag{34}$$

The approach is similar for left propagating solutions, except initial values are imposed at the left endpoint and $ik_r$ is replaced by $-ik_l$. Once the solution vector, $\hat{\mathbf{u}}$ is computed, the reflection and tunneling probabilities are calculated by

$$R(\lambda) = \left| \frac{(ik_l\boldsymbol{\delta}_- - \boldsymbol{\nu}_-)\hat{\mathbf{u}}}{(ik_l\boldsymbol{\delta}_- + \boldsymbol{\nu}_-)\hat{\mathbf{u}}} \right|^2, \quad T(\lambda) = 1 - R(\lambda) \tag{35}$$

## V. NUMERICAL INNER PRODUCTS

Frequently in quantum mechanics, one is interested in computing inner products such as a transition probability or the expectation value of an operator. Here we show that when the spectral-tau method is used to compute the expansion coefficients for the eigenfunctions of the Hamiltonian, inner products can be computed rapidly with quadrature accuracy without requiring a transformation to point space. Now supposing one wishes to compute the inner product

$$\langle u|v\rangle = \int_{-1}^{+1} u^*(x)v(x)dx \tag{36}$$

The numerical integration is carried out as

$$\langle u|v\rangle = \mathbf{b}\hat{\mathbf{U}}^\dagger\hat{\mathbf{v}} \tag{37}$$

Here the notation $\hat{\mathbf{U}}^\dagger$ does not mean the Hermitian conjugate of the matrix $\hat{\mathbf{U}}$, but rather that the matrix is constructed using the complex conjugates of the elements of $\hat{\mathbf{u}}$. The definite integral operator $\mathbf{b}$ is

$$\mathbf{b} = -2\left(\begin{array}{cccccccc} -1 & 0 & 3^{-1} & 0 & 15^{-1} & 0 & \cdots & (N^2-1)^{-1} \end{array}\right) \tag{38}$$

Constructing the convolution matrix is the most numerically expensive aspect since it scales as $O(N^3)$. This can be improved greatly by plugging the definition into the inner product.

$$\langle u|v\rangle = \mathbf{b}\sum_{k=0}^{N} \hat{u}_k^*\mathbf{T}_k\hat{\mathbf{v}} = \sum_{k=0}^{N} \hat{u}_k^*\mathbf{b}\mathbf{T}_k\hat{\mathbf{v}} \tag{39}$$

On can then define an inner product operator matrix where the rows are the integrated convolution matrices of the basis functions

$$\mathbf{K} = \begin{pmatrix} \mathbf{b}\mathbf{T}_0 \\ \mathbf{b}\mathbf{T}_1 \\ \vdots \\ \mathbf{b}\mathbf{T}_N \end{pmatrix} \tag{40}$$

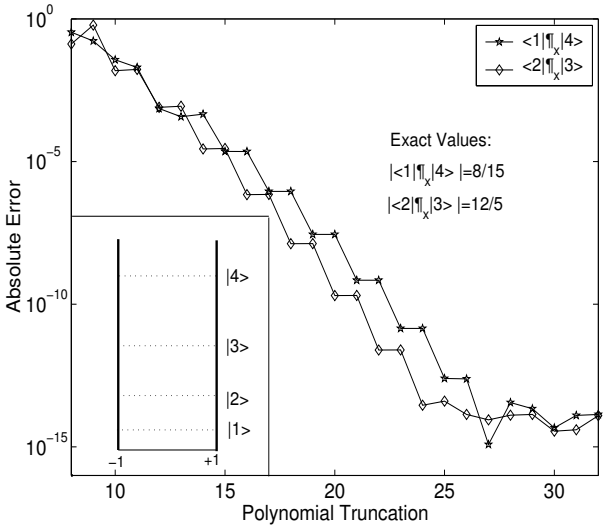


FIG. 8: Convergence of the transition matrix elements of the scaled momentum operator.

The benefit to constructing the matrix $\mathbf{K}$ is that it may be computed to an arbitrarily large truncation, independent of a given problem. This matrix can be stored in a file and one need only take the upper left $(N+1)\times(N+1)$ sub-matrix to compute the inner product. One then has

$$\langle u|v\rangle = \hat{\mathbf{u}}^*\mathbf{K}\hat{\mathbf{v}} \tag{41}$$

Where $\mathbf{u}^*$ is the Hermitian conjugate. One is also frequently interested in computing a number of transition probabilities or expectation values of operators. Given a linear operator $\hat{\mathcal{O}}$ which is discretized as $\mathbf{O}$, it is possible to compute transition probabilities between a number of states $u_j$ where $j = 1...n$ simultaneously. Let $\mathbf{S}$ be a an $(N+1)\times n$ matrix containing a subset of the eigenvectors of the discretized Hamiltonian $\mathbf{H}$ such that

$$\mathbf{S} = \left(\begin{array}{cccccc} \hat{\mathbf{u}}_1 & \hat{\mathbf{u}}_2 & \hat{\mathbf{u}}_3 & \cdots & \hat{\mathbf{u}}_n \end{array}\right) \tag{42}$$

Then the complete transition matrix for the operator $\mathcal{L}$ is

$$\begin{pmatrix} \langle u_1|\hat{\mathcal{O}}u_1\rangle & \langle u_1|\hat{\mathcal{O}}u_2\rangle & \cdots & \langle u_1|\hat{\mathcal{O}}u_n\rangle \\ \langle u_2|\hat{\mathcal{O}}u_1\rangle & \langle u_2|\hat{\mathcal{O}}u_2\rangle & & \langle u_2|\hat{\mathcal{O}}u_n\rangle \\ \vdots & & \ddots & \vdots \\ \langle u_n|\hat{\mathcal{O}}u_1\rangle & \langle u_n|\hat{\mathcal{O}}u_2\rangle & \cdots & \langle u_n|\hat{\mathcal{O}}u_n\rangle \end{pmatrix} = \mathbf{S}^*\mathbf{K}\mathbf{O}\mathbf{S} \tag{43}$$

The matrix $\mathbf{KO}$ can be prepared in advance, since it does not depend on the potential. With this advantage, the matrix multiplication in the spectral domain is as fast as the analogous computation in point space. One benefit of working in the spectral domain is that it is easy to determine if a solution if fully resolved by observing the exponential decay of expansion coefficients. This is less apparent by examining the solution's behavior in point space.

## VI. CONCLUDING REMARKS

We have presented a fast and efficient method of solving the TISE for an arbitrary semiconductor heterostructure. By expanding in terms of orthogonal polynomials, we obtain a matrix representation of the Hamiltonian from which we may simultaneously compute as many eigenfunctions and eigenvalues as desired. This offers a substantial advantage over more prevalent shooting methods as we do not need to hunt for eigenvalues because that work is performed by a matrix eigen-solver routine. For all examples, the MATLAB®function `eig` was used to obtain eigenvalues and eigenvectors. We have also shown that the spectral method requires much smaller matrices than the finite difference method to achieve comparable error. Frequently, the spectral matrix size is orders of magnitude smaller. Integration preconditioning was introduced to the Schrödinger eigenproblem, giving a sparse quasi-banded structure to the matrices.

The spectral element method was then extended to incorporate unbounded domains through rational mapping. The mapping demonstrated superior convergence over the more traditional domain truncation approach. We discussed the phenomena of resonances and the difficulties of computing them. Using a complex coordinate deformation for the end elements, we showed that one may solve the TISE on a new contour, along which its eigenfunctions have a convergent expansion. Additionally, the scattering states and tunneling probability were shown to be easily obtainable by formulating a spectral element initial value problem. Finally we demonstrated that one may easily compute inner products and expectations of operators in the spectral domain using simple matrix vector multiplication.

### Acknowledgements

This work supported by DOE Basic Energy Sciences Grant DE-FG03-02ER46014 and DOE SNL Grant 66513

[1] C. Canuto, M. Y. Hussaini, A. Quarteroni, and T. A. Zang, *Spectral Methods in Fluid Dynamics*, Springer-Verlag, New York (1987)
[2] T. Shibata, Phys. Rev B. **43** (8) 6760-6763 (1991)
[3] A. Peres, J. Math. Phys **24** 1110-1119 (1983)
[4] M. Čížek, J. Horáček, J. Phys. A, **29** 6325-6342 (1996)
[5] A. F. M. Anwar and M. M. Jahan, Phys. Rev. B, **50** (15) 10864-10867 (1994)
[6] P. Midy, O. Atabek, and G. Oliver J. Phys. B: At. Mol. Opt. Phys **26** 835-853 (1993)
[7] M. Braun, S.A. Sofianos, D.G. Papageorgiou, and I.E. Lagaris J. Comp. Phys. **126** 315-327 (1996)
[8] C. Lanczos, *Applied Analysis*, Prentice-Hall, Englewood Cliffs, NJ, (1956).
[9] G. H. Golub, C. F. van Loan, *Matrix Computations* Johns Hopkins University Press (1996).
[10] D. Gottlieb and S. Orszag, *Numerical Analysis of Spectral Methods*, SIAM, Philadelphia, PA (1977).
[11] G. Szegö, *Orthogonal Polynomials*, American Mathematical Society Colloquium Publications, Vol 23, (2003)
[12] B. Fornberg *A Practical Guide to Pseudospectral Methods*, Cambridge University Press (1998)
[13] D. Gottlieb and C.W. Shu, SIAM Rev. **39** 644-668 (1997)
[14] E.A. Coutsias, T. Hagstrom, D. Torres, Math. Comp., **65**, (214) 611-635
[15] E.A. Coutsias, T. Hagstrom, J.S. Hesthaven, and D. Torres, Proc. of International Conference on Spectral and High Order Methods, ICOSAHOM '95, Houston, USA, 1995, pp. 21-38
[16] R.B. Lehoucq, D.C. Sorensen, and C. Yang, *ARPACK Users' Guide: Solution of Large-Scale Eigenvalue Problems with Implicitly Restarted Arnoldi Methods*, SIAM (1998)
[17] I. Alonso-Mallo and N. Reguera, SIAM J. Numer. Anal. **40** (1) 134-158 (2002)
[18] F. Tisseur and K. Meerbergen, SIAM Rev **43** (2) pp. 235-286 (2001)
[19] J. Shen, SIAM J. Numer. Anal. **38** (4) 1113-1133 (2000)
[20] H. I. Siyyam, J. Comp. Anal. App., **3** (2) 173-182 (2001)
[21] B. Guo, J. Shen, Z. Wang, Int. J. Num. Meth.Eng. **53** 65-84 (2002)
[22] H. V. McIntosh, "Quantization as an Eigenvalue Problem" in *Group Theory and its Applications*, (E.M. Loebl, ed.), Academic Press, New York, (1975)
[23] R. de la Madrid and M. Gadella, Am. J. Phys. **70** 626-638 (2002)
[24] E. Hernández, A. Jáuregui, and A. Mondragón, Phys. Rev. A **67** 022721 (2003)
[25] U. Leonhardt and S. Schneider, Phys. Rev. A **56**, (4) 2549-56 (1997)
[26] E. N. Economou, *Green's Functions in Quantum Physics* Springer-Verlag (1983)
[27] G. Barton, *Elements of Green's Functions and Propagation: Potentials, Diffusion, and Waves* Oxford Univ Press (1989)
[28] W. P. Rheinhard, Ann. Rev. Phys. Chem., **33** 223-255 (1982)
[29] M. F. Levy, Proc. Roy. Soc. Lond. A, **457**, 2609-2624 (2001)
[30] Hagstrom, T., "New results on absorbing layers and radiation boundary conditions", in *Topics in Computational Wave Propagation*, M. Ainsworth, P. Davies, D. Duncan, P. Martin, and B. Rynne, eds., Springer-Verlag, (2003), 1-42.

## APPENDIX A: CHEBYSHEV MATRICES AND MATLAB®SCRIPTS

The fast cosine transform from nodal to spectral values is

```
temp=ifft([u(1:N);u(N-1:-1:2)]);
uhat=[temp(1,:); 2*temp(2:N,:)];
```

and the transform from spectral to nodal values is

```
temp=fft([uhat(1,:); ...
[uhat(2:N,:);uhat(N-1:-1:2,:)]/2]);
u=temp(1:N,:);}
```

The Chebyshev differentiation matrix, $\mathbf{D}$, for $N = 8$ is

$$\mathbf{D} = \begin{pmatrix} 0 & 1 & 0 & 3 & 0 & 5 & 0 & 7 & 0 \\ 0 & 0 & 4 & 0 & 8 & 0 & 12 & 0 & 16 \\ 0 & 0 & 0 & 6 & 0 & 10 & 0 & 14 & 0 \\ 0 & 0 & 0 & 0 & 8 & 0 & 12 & 0 & 16 \\ 0 & 0 & 0 & 0 & 0 & 10 & 0 & 14 & 0 \\ 0 & 0 & 0 & 0 & 0 & 0 & 12 & 0 & 16 \\ 0 & 0 & 0 & 0 & 0 & 0 & 0 & 14 & 0 \\ 0 & 0 & 0 & 0 & 0 & 0 & 0 & 0 & 16 \\ 0 & 0 & 0 & 0 & 0 & 0 & 0 & 0 & 0 \end{pmatrix} \tag{A1}$$

This can be constructed easily with the script

```
D=zeros(N+1);
for k=1:N D(k,k+1:2:N+1)=2*(k:2:N) end
D(1,:)=D(1,:)/2;
```

The Chebyshev position operator matrix is

$$\mathbf{X} = \frac{1}{2} \begin{pmatrix} 0 & 1 & 0 & & & \\ 2 & 0 & 1 & 0 & & \\ 0 & 1 & 0 & 1 & 0 & \\ & 0 & 1 & 0 & 1 & 0 \\ & & & \ddots & & \ddots \end{pmatrix} \tag{A2}$$

The $\mathbf{X}$ matrix has the script

```
band=ones(N,1)/2;
X=diag(band,-1)+diag(band,1);
X(2,1)1=1;
```

The Chebyshev integration matrix, $\mathbf{B}$, which is the pseudo-inverse of $\mathbf{D}$ has the form

$$\mathbf{B}_{[1]} = \begin{pmatrix} 0 & 0 & 0 & 0 & 0 & \dots & 0 \\ 1 & 0 & -\frac{1}{2} & 0 & 0 & \dots & 0 \\ 0 & \frac{1}{4} & 0 & -\frac{1}{4} & 0 & \dots & 0 \\ \vdots & & \ddots & \ddots & \ddots & & \vdots \\ \vdots & & & \frac{1}{2i} & 0 & -\frac{1}{2i} & \\ \vdots & & & & \ddots & \ddots & \vdots \\ 0 & & \dots & & & \frac{1}{2N} & 0 \end{pmatrix} \tag{A3}$$

The script for the $\mathbf{B}_{[1]}$ matrix is

```
band=[0 1./(2*(1:N+1))];
B=diag(band(2:N+1),-1)-diag(band(1:N),1);
B(2,1)=1;
```

The Dirichlet and Neumann operators are

$$\begin{aligned} \boldsymbol{\delta}_- &= \begin{pmatrix} 1 & -1 & 1 & -1 & 1 & -1 & \cdots & (-1)^N \end{pmatrix} \\ \boldsymbol{\delta}_+ &= \begin{pmatrix} 1 & 1 & 1 & 1 & 1 & 1 & \cdots & 1 \end{pmatrix} \\ \boldsymbol{\nu}_- &= \begin{pmatrix} 0 & 1 & -4 & 9 & -16 & 25 & \cdots & N^2(-1)^{N+1} \end{pmatrix} \\ \boldsymbol{\nu}_+ &= \begin{pmatrix} 0 & 1 & 4 & 9 & 16 & 25 & \cdots & N^2 \end{pmatrix} \end{aligned} \tag{A4}$$